# Cannabis compounds have anti-inflammatory activity in lung epithelial cells but pro-inflammatory activity in macrophages while increasing phagocytosis *in vitro*

**Seegehalli M Anil**
ARO, Volcani Center
**Nurit Shalev**
ARO, Volcani Center
**Ajjampura C Vinayaka**
ARO, Volcani Center
**Stalin Nadarajan**
ARO, Volcani Center
**Dvory Namdar**
ARO, Volcani Center
**Eduard Belausov**
ARO, Volcani Center
**Irit Shoval**
Bar Ilan University
**Karthik Ananth Mani**
ARO, Volcani Center
**Guy Mechrez**
ARO, Volcani Center
**Hinanit Koltai** ( hkoltai@agri.gov.il )
ARO, Volcani Center

**Research Article**

**Keywords:** cannabis, covid-19, cannabinoids, terpenes, interleukin, chemokine, macrophages, epithelial cells, lung, inflammation

**Posted Date:** October 8th, 2020

**DOI:** https://doi.org/10.21203/rs.3.rs-89166/v1

**Version of Record:** A version of this preprint was published at Scientific Reports on January 14th, 2021.
See the published version at https://doi.org/10.1038/s41598-021-81049-2.

# Abstract

*Cannabis sativa* is widely used for medical purposes and has anti-inflammatory activity. The purpose of this study was to examine the anti-inflammatory activity of cannabis on markers of immune responses associated with Coronavirus disease 2019 (COVID-19) inflammation. An extract fraction from *C. sativa* Arbel strain ($F_{CBD}$) substantially reduced dose dependently interleukin (IL) 6 and 8 levels in an alveolar epithelial (A549) cell line. $F_{CBD}$ contained cannabidiol (CBD), cannabigerol (CBG) and tetrahydrocannabivarin (THCV), and multiple terpenes. Treatments with $F_{CBD}$ and phytocannabinoid standards that compose $F_{CBD}$ ($F_{CBD:std}$) reduced IL-6, IL-8, *C-C Motif Chemokine Ligands* (*CCLs*) 2 and 7, and *angiotensin I converting enzyme 2* (*ACE2*) expression in the A549 cell line. Treatment with $F_{CBD}$ induced macrophages (differentiated KG1 cell line) polarization and phagocytosis *in vitro*, and increased *CD36* and *type II receptor for the Fc region of IgG* (*FcγRII*) expression. $F_{CBD}$ treatment also substantially increased *IL-6* and *IL-8* expression in macrophages. $F_{CBD:std}$, while maintaining the anti-inflammatory activity in alveolar epithelial cells, led to reduced phagocytosis and pro-inflammatory IL secretion in macrophages in comparison to $F_{CBD}$. The phytocannabinoid mixture may show superior activity versus cannabis fraction for reduction of lung inflammation, yet there is a need of caution in proposing cannabis as treatment for COVID-19.


# Introduction

Coronavirus disease 2019 (COVID-19) is an acute resolved disease following infection by SARS-CoV-2 with a mortality of ~3.7%. Respiratory failure due to acute respiratory distress syndrome is the leading cause of mortality[1]. Disease progression of COVID-19 is often characterized by a two-phase immune responses. A specific adaptive immune response is required at the first phase to eliminate the virus and to prevent disease progression to severe stages[2]. Therefore, strategies to increase immune responses at this first stage are critical.

The second phase is usually associated with a virally induced cytokine storm syndrome[1-2]. The cytokine storm syndrome is characterized by elevated levels of several cytokines including interleukin 6 (IL-6) and interleukin 8 (IL-8), tumor necrosis factor (TNF) and C-C Motif Chemokine Ligand 2 (CCL2)[3]. Specific to the respiratory system, lung epithelial cells were suggested to play a crucial role in the release of several pro-inflammatory cytokines such as IL-6 and IL-8[4].

*Cannabis sativa* is widely used for medical purposes worldwide. Cannabis strains produce more than 500 compounds, including phytocannabinoids, terpenes and flavonoids[5-7]. Cannabinoids were previously suggested to be immune modulators and to change the balance between pro- and anti-inflammatory cytokines[8-9]. Cannabinoids also influence macrophage activity. For example, Δ9-tetrahydrocannabivarin (THCV) inhibited nitrite production and interleukin 1β (IL-1β) protein levels in lipopolysaccharide activated macrophages[10]. Further, Δ9-tetrahydrocannabinol (THC) was shown to inhibit macrophages

phagocytosis by 90%[11]. However, little is known regarding the effect of different cannabis compounds and their combinations on alveolar epithelial and immune cell inflammation.

Here, we identified cannabis compounds that have anti-inflammatory activity in lung epithelial cells, yet substantially induce polarization, phagocytosis and IL expression in macrophages *in vitro*.

# Results

### Cannabis crude extract and fractions reduce the level of IL-8 and IL-6 in lung epithelial cell model

The high CBD cannabis strain Arbel was used to examine extract activity in reducing inflammation induced by TNFα in the lung epithelial cancer cell line A549. The crude extract led to a substantial reduction of IL-6 and IL-8 secretion levels at 5 µg/mL (Fig. 1A,B). Subsequently, high CBD ($F_{CBD}$) and high THC ($F_{THC}$) fractions were examined for their anti-inflammatory activity (Fig. 1A, Supplementary Fig. S1). $F_{THC}$ exhibited only low anti-inflammatory activity; however, $F_{CBD}$ showed considerable activity in the reduction of IL-6 and IL-8 secretion levels from lung epithelial cells, with $IC_{50}$ of 3.45 and 3.49 µg/mL, respectively (Fig. 1C,D). $F_{CBD}$ activity was greater than that of dexamethasone at 4 µg/mL for reducing IL-8 levels, and similar to that of the crude extract for reducing both IL-6 and IL-8 levels (Fig. 1A,B). Crude extract and $F_{THC}$ led to substantial cell death, whereas $F_{CBD}$ at 5 µg/mL was comparatively less cytotoxic (76.7% viability; Supplementary Fig. S2).

CBD (the main phytomolecule in $F_{CBD}$) alone showed a bell shaped activity curve, i.e., 3.0 µg/mL showed anti-inflammatory activity for both IL-6 and IL-8 levels, similar to $F_{CBD}$ at 4.1 µg/mL (Fig. 2 A,B). Nevertheless, higher or lower concentrations of CBD had lower and/or non-significant activity in reducing IL-6 and IL-8 levels (Fig. 2 A,B).

### $F_{CBD:std}$ showed activity similar to $F_{CBD}$ in lung epithelial cell model

Based on HPLC and GC/MS analysis, $F_{CBD}$ contains approximately66%  phytocannabinoid by total content. The phytocannabinoid assemblage included CBD (93.5%), CBG (6.1%) and minute amount of THCV (0.4%) (Supplementary Fig. S1). Multiple terpenes were detected in $F_{CBD}$ (Table 1; Supplementary Fig. S3). The combination of phytocannabinoid standards at the ratio found in fraction $F_{CBD}$ ($F_{CBD:std}$) resulted in activity similar to that of the initial fractions ($IC_{50}$ of 4.1 µg/mL for IL-6 and IL-8; Fig. 1E,F).

| Compound | % of terpenes | % of total |
|---|---|---|
| Butylated hydroxytoluene | 2.6 | 0.3 |
| 1,6-Dioxacyclododecane-7,12-dione | 1 | 0.1 |
| Guaiol | **10.4** | **1.2** |
| γ-Eudesmol | 2.3 | 0.3 |
| α-Eudesmol | 5.6 | 0.6 |
| Guaienol | 1.3 | 0.2 |
| γ-Curcumene | **75.6** | **8.7** |
| other | 1.2 | 0.1 |

**Table 1.** Chemical composition of fraction $F_{CBD}$ analyzed using gas chromatography coupled with mass spectrometer (GC-MS). Relative amounts of terpenes, terpenoids and cannabinoids are given.

### CB2 inverse agonist attenuated $F_{CBD}$ and $F_{CBD:std}$ activity in lung epithelial cell model

Using CB2 receptor inverse agonists (IA) with $F_{CBD}$ or $F_{CBD:std}$ treatments led to reduced activity of the fraction and standard mix against IL-6 and IL-8 secretion in A549 cells (Fig. 3A,B). However, treatment with CB1 IA or a TRPA1 blocker did not affect $F_{CBD}$ or $F_{CBD:std}$ activity. Treatment with CB1 or CB2 IA led only to reduction in IL-6 and IL-8 levels in these cells, CB1 to a greater extent (Fig. 3A,B).

### $F_{CBD}$ treatment lead to reduction in *CCL2*, *CCL7*, *ACE2* and *IL-7* gene expression in lung epithelial cell model

qPCR analysis demonstrated that $F_{CBD}$ or $F_{CBD:std}$ treatments reduced the steady state level of mRNA of the pro-inflammatory cytokines *CCL2* and *CCL7* in TNFα treated A549 cells, determined with *HPRT1* as a reference gene (Fig. 4A,B). However, the reduction in expression of the two genes was less than that of dexamethasone (Fig. 4A,B). $F_{CBD:std}$ treatment led to only a minor reduction in the expression level of *IL-7*, whereas $F_{CBD}$ and dexamethasone reduced *IL-7* expression substantially (Fig. 4C). Moreover, $F_{CBD}$ or $F_{CBD:std}$ treatments reduced the expression level of *ACE2*, $F_{CBD}$ to a greater extent than dexamethasone or $F_{CBD:std}$ (Fig. 4D).

### $F_{CBD}$ and $F_{CBD:std}$ treatments induce *IL-6*, *IL-8* and *CCL2* expression in differentiated KG1 cell line

$F_{CBD}$ treatment increased *IL-6*, *IL-8* and *CCL2* expression in PMA-treated (differentiated KG1 cells) macrophages by ~2, ~433 and ~49 fold, respectively (Fig. 5A,B,C). $F_{CBD:std}$ increased *CCL2* expression by ~20 fold (Fig. 5C) and *IL-8* expression level by ~26 fold, however $F_{CBD:std}$ did not lead to an increase in *IL-6* expression level in macrophages (Fig. 5A,B,C). At the protein level in KG1 treated with TNFα, $F_{CBD}$ but not $F_{CBD:std}$ increased IL-8 secretion in macrophages (Fig. 5D). $F_{CBD}$ was dose dependent (Fig. 5E). Dexamethasone (at 8 or 4 µg/mL) did not decrease expression of *IL-6*, *IL-8*, *CCL2, IL-8* or IL-8 secretion in macrophages (Fig. 5A,B,C and Fig. 5D,E, respectively).

### $F_{CBD}$ and $F_{CBD:std}$ attenuate macrophages polarization

To examine the effect of the treatments on macrophage phagocytosis activity we incubated PMA-treated macrophages with SNP or SNPG. In the control (vehicle treated), most of the cells were non-polarized and featured a round structure (Table 2; Fig. 6), whereas the macrophage population treated for 16 h with $F_{CBD}$ (7 µg/mL) consisted of ~48 % polarized cells (Table 2). Multiple silica particles and membrane pseudopods were detected in these polarized cells (Fig. 6). Likewise, treatment of the macrophage population with $F_{CBD:std}$ resulted in ~49 % polarized cells (Table 2). Accordingly, lower concentrations of $F_{CBD}$ (3.5 µg/mL) led to a somewhat reduced percentage of polarized cells (~45 %) and treatment of macrophages with CBD at the relevant concentration (4.35 µg/mL) as in $F_{CBD}$ 7 µg/mL resulted in only ~18 % polarized cells.

| Treatment | % of polarized cells | Total number of cells counted in all replicates (n = 5) |
|---|---|---|
| control | $1.2 \pm 0.83^{b}$ | 204 |
| $F_{CBD}$ (7 µg/mL) | $48.3 \pm 6.9^{a}$* | 144 |
| $F_{CBD\text{-}std}$ (7 µg/mL) | $48.8 \pm 11.3^{a}$* | 74 |
| CBD (4.3 µg/mL) | $17.9 \pm 4.1^{ab}$* | 94 |
| $F_{CBD}$ (3.5 µg/mL) | $44.9 \pm 12.4^{a}$* | 70 |

**Table 2.** Percentage of polarized cells out of total cells of differentiated KG1 cell population that were counted in n = 5. Control, vehicle control; $F_{CBD+THC}$, $F_{CBD}$ with 3% THC; $F_{CBD\text{-}std}$, CBD (93.5%), CBG (6.1%) and THCV (0.4%). Means with different letters are significantly different from all combinations of pairs by Tukey-Kramer honest significant difference (HSD; $P \leq 0.05$). ***,** Mean significantly different from control based on Student T-test ($P \leq 0.05$).

### $F_{CBD}$ and $F_{CBD:std}$ attenuate expression of phagocytosis-associated receptors

$F_{CBD}$ treatment but not $F_{CBD:std}$ increased expression of *FcγRII* and *CD36*, in comparison to the vehicle control (Fig. 7A,B). Treatment with Ruxolitinib which inhibits monocyte activation[12] reduced *FcγRII* expression (Fig. 7A), and PA reduced expression of *CD36* (Fig. 7B), in agreement with[13]. Expression of *SCARB1* was reduced by $F_{CBD}$ and Roxulitinib but not by $F_{CBD:std}$ (Fig. 7C).

### $F_{CBD}$ increase internalization of silica particles in macrophages

Based on cell analysis by Imaging Flow Cytometry for macrophages with internalized silica particles, it was found that $F_{CBD}$ increased the percentage of cells that internalized fluorescent-labeled silica particles (SNP, Table 3; Supplementary Fig. S4). The increase in percentage of positive cells by $F_{CBD}$ was higher in comparison to the vehicle control also for the smaller fluorescent-labeled silica particles, ENP and ENPG. $F_{CBD:std}$ and CBD treatments were less effective in increasing of internalization (for SNP) or presence (ENP and ENPG) of the particles in cells in comparison to the $F_{CBD}$ treatment (Table 3; Supplementary Fig. S4).

| ENPG | ENP | SNP | Treatment |
|---|---|---|---|
| $100.0^{a}$ | $100.0^{a}$ | $100.0^{b}$ | control |
| $132.9 \pm 30.3^{a}$ | $167.9 \pm 11.2^{a}$* | $147.8 \pm 13.4^{a}$ | $F_{CBD}$ |
| $116.2 \pm 3.1^{a}$* | $125.3 \pm 10.2^{a}$ | $99.8 \pm 0.8^{b}$ | $F_{CBD:std}$ |
| $89.6 \pm 3.9^{a}$ | $121.3 \pm 24.0^{a}$ | $118.85 \pm 5.10^{ab}$ | CBD |

**Table 3. Percentage of macrophage cells with internalization of SNP silica beads or positive for ENP or ENPG silica beads analyzed using Imaging Flow Cytometry following treatment with $F_{CBD}$ at 7 µg/mL, $F_{CBD:std}$ at 7 µg/mL, CBD at 4.35 µg/mL and solvent (vehicle) control.** Differentiated KG1 cells were treated with the above treatments for 16 h and then incubated with 40 µg/mL Fluorescein labeled silica beads (50-100 nm [SNP], 30-70nm [ENP] or 30-70nm coated with IgG [ENPG]) for 4 h. At least 4,000-6,000 cells for each treatment were analyzed using the Amnis IDEAS software and the distribution of the cell internalization scores were plotted (n=2). Means with different letters are significantly different from all combinations of pairs by Tukey-Kramer`s honest significant difference (HSD; $P \leq 0.05$). *indicates significantly different mean from the control based on Student T-test ($P \leq 0.05$).

# Discussion

We have identified CBD rich fraction ($F_{CBD}$) from the inflorescence extract of a high CBD cannabis strain with immune-modulation activity in alveolar epithelial and macrophage cell models. $F_{CBD}$ reduced IL-8 and IL-6 secretion in alveolar epithelial cells. IL-8 is one of the cytokines that characterizes the cytokine storm in severe COVID-19 patients; IL-6 is a prominent cytokine also involved in the cytokine storm and is secreted during the disease from alveolar epithelial cells[3]. In addition to CBD, $F_{CBD}$ contained CBG and minute amount of THCV. $IC_{50}$ of the combinations of active standards ($F_{CBD:std}$) at the relative concentrations found in the original fraction were similar to that of $F_{CBD}$ in the alveolar epithelial cell model.

Treatment with CBD by itself led to a reduction in IL-6 and IL-8 levels in a bell-shaped dose-response in alveolar epithelial cells; i.e., only 3 µg/mL was active whereas other CBD concentrations exhibited lower or no cell activity. These results are in line with the earlier publication suggesting that CBD has a bell-shaped dose-response for anti-inflammatory activity[14]. Notably, $F_{CBD}$ (i.e., combination of CBD with CBG and THCV) led to a dose-dependent response rather than a bell-shaped dose-response. These results are in accordance with [14], suggesting that the addition of other phytomolecules to CBD (crude cannabis extract in the case of [14]) prevented its bell-shaped dose-response. The CBD bell-shaped dose-response is associated with a narrow therapeutic window, which is difficult to use effectively in clinical therapy. Therefore, the fact that $F_{CBD}$ has a dose-dependent response makes it better suited than CBD for patient care.

CBD is a negative allosteric modulator of CB1 signaling[15]. TRPA1 is a receptor in alveolar epithelial cells involved in the pathogenesis of several airway diseases including chronic obstructive pulmonary disease and asthma[16]. Nevertheless, co-treatment with inverse agonists for CB2 only had an effect on $F_{CBD}$ or $F_{CBD:std}$ activity. Treatment with CB1 IA or TRPA1 blocker had no effect. Hence, this anti-inflammatory activity may be mediated, at least partially, *via* the CB2 receptor. Nevertheless, the involvement of CB receptors in $F_{CBD}$ or $F_{CBD:std}$ activity still needs to be demonstrated and additional studies should be conducted to prove this suggested association.

In addition to reducing IL-6 and IL-8 levels, $F_{CBD}$ and $F_{CBD:std}$ reduced the expression level of *CCL2* and *CCL7* in alveolar epithelial cells induced with TNFα. The systemic cytokine profiles detected in severe COVID-19 patients includes increased production of inflammatory chemokines such as CCL2[17]. Moreover, CCL2 and CCL7 were shown to be abundant in bronchoalveolar fluid from severe COVID-19 patients and were associated with recruitment of monocytes into the lungs[17]. Our results suggest that treatment with $F_{CBD}$ or $F_{CBD:std}$ may lead to reduced secretion of inflammatory cytokines associated with the disease, and possibly to a reduction of macrophage recruitment during the cytokine storm. However, dexamethasone was more effective than $F_{CBD}$ in reducing both *CCL2* and *CCL7* expression.

IL-7 was shown to raise lymphocyte counts in septic patients with low absolute lymphocyte counts[18] and to restore protective immunity in patients that suffer from CD4+ T cell deficiency (e.g., as in the case of

HIV infection[19]). It was suggested that treatment against SARS-CoV-2 infection should also attempt to increase IL-7 levels[18]. The fact that $F_{CBD:std}$ reduced *IL-7* expression only to a minor extent in comparison to dexamethasone or $F_{CBD}$ suggests that using purified phytocannabinoids may have an advantage over cannabis-derived fractions for COVID-19-like inflammation.

$F_{CBD}$ reduced the expression level of *ACE2*, and $F_{CBD:std}$ and dexamethasone also reduced its expression but to a lesser extent. The ACE-2 receptor is a part of the dual renin-angiotensin system[20]. ACE-2 was shown to be involved with SARS-CoV-2 human infection ; the ectodomain of the S protein of SARS-CoV binds to the peptidase domain of ACE2 with relatively high affinity[21]. In cells of patients with severe symptoms of COVID-19, ACE2 was substantially upregulated 199 fold; this upregulation was suggested to be one of the factors leading to disruption of the renin-angiotensin system[22]. The ability of $F_{CBD}$ to reduce *ACE2* expression is important concerning treatment of COVID-19 patients, yet should be considered with care as the advantages and disadvantages of *ACE2* expression reduction are disputed[20].

In the first phase of the disease, a specific adaptive immune response is needed to eliminate the virus and to prevent disease progression to more severe stages[2]. Indeed, the dysfunction of alveolar macrophages are among the abnormal characteristics in some severe COVID-19 patients[23], and an abundance of increased inflammatory monocyte-derived macrophages replaces tissue-resident alveolar macrophages in patients with severe disease[24]. In addition, during SARS-CoV-1 infections that provoke a disease course similar to those seen during infection with SARS-CoV-2[24], a marked reduction in phagocytosis by macrophages was detected[25]. Also, phagocytosis was important in the antibody-mediated elimination of SARS-CoV-1 in a mouse model[26].

Notably, $F_{CBD}$ and $F_{CBD:std}$, and CBD to a lesser extent, led to a marked increase in macrophage polarization and to cell actin remodeling that corresponds to the growth of membrane filopodia-like structures[27]. $F_{CBD}$ reduced expression of *SCARB1*; *SCARB1* encodes SR-B1 that is a scavenger receptor (class B) also is responsible for phagocytosis of silica particles in macrophages[28]. However, $F_{CBD}$ treatment also led to an increase in *FcγRII* and *CD36* gene expression. Phagocytosis is initiated by ligation of Fcγ receptors to IgG-opsonins on the target cell[29], whereas CD36 expression in macrophages was shown to be involved with lung fibrosisin in mice[30]. Alveolar macrophages play an important role in Fc receptor-mediated responses during acute virus infections and in phagocytosis-mediated clearance of respiratory virus infections[31-32]. CD36 is an important scavenger receptor for phagocytosis of *Streptococcus pneumoniae*, a primary bacterial agent associated with pneumonia, which is down regulated by influenza[33]. Indeed, $F_{CBD}$ led to a marked increase in the internalization of silica particles by macrophages, and in so doing, to increased levels of phagocytosis.

Possibly, the increase in macrophage polarization and phagocytosis, and the upregulation of expression of *FcγRII* and *CD36* in these cells following $F_{CBD}$ treatment may facilitate phagocytosis-mediated clearance of respiratory viruses, and benefit the first phase of the immune response to SARS-CoV-2.

However, it should be noted that macrophages themselves can be infected by the virus, as SARS-CoV-1 infect macrophages as a result of IgG-mediated phagocytosis that requires FcγRII receptor signaling pathways[34]. Advantages and disadvantages of increasing macrophage phagocytosis activity should be carefully considered[3,35].

Notably, although $F_{CBD:std}$ treatment increased macrophage polarization, it did not increase the phagocytosis-associated gene expressions, nor phagocytosis. Hence, additional active compounds in the cannabis-derived $F_{CBD}$ and not in the phytocannabinoid standard mix that composed $F_{CBD:std}$ are responsible for this increased gene expression and phagocytosis activity. Indeed, $F_{CBD}$ contained multiple terpenes, some of them such as γ-Curcumene or Guaiol at considerable percentages. The presence of terpenes in $F_{CBD}$ may account for the differences in activity between $F_{CBD}$ and $F_{CBD:std}$.

During the second phase of COVID-19, pneumonia patients exhibit features of macrophage activation syndrome (MAS) in which macrophages play a major pro-inflammatory role by releasing pro-inflammatory cytokines such as IL-6, IL-8 and CCL2[3]. Moreover, subsets of macrophages in patients with COVID-19 were found to express genes associated with IL-6, whereas expression of IL-6 was again associated with severe depletion of lymphocytes from the spleen and lymph nodes[35]. Notably, $F_{CBD}$ led to a marked increase of *IL-8* expression levels in macrophages, IL-8 protein levels and to increase in *IL-6* expression levels, above that induced by PMA[36]. These results suggest a substantial, *in vitro*, pro-inflammatory role for $F_{CBD}$ in macrophages. However, $F_{CBD;std}$ was less active in ILs induction, again demonstrating a notable difference between $F_{CBD}$ and $F_{CBD:std}$, which may originate from the presence or absence, respectively, of terpenes.

To conclude, treatment with cannabis compounds CBD, CBG and THCV may have clinical value in reducing cytokine secretion and *ACE2* expression in lung epithelial cells. However, treatment with $F_{CBD}$ containing terpenes in addition to phytocannabinoids substantially induced macrophage phagocytosis and increased their ILs levels. These results suggest a pro-inflammatory role for cannabis preparation that is higher than that of the phytocannabinoid standard mix only. The latter maintained the anti-inflammatory activity in alveolar epithelial cells with relatively reduced pro-inflammatory activity in macrophages. Hence, the mix of phytocannabinoids shows superior activity versus the cannabis-derived fraction. Nevertheless, there is a need of caution in proposing cannabis treatment for COVID-19, as is presently being suggested in the media. Increase of macrophage-secreted IL-6 and IL-8 levels by cannabis-based treatment may potentially lead to worsening of the "cytokine storm" identified in severe COVID-19 patients. It should be stressed, in agreement with[37], that as for now, users and healthcare personnel should avoid the use of cannabis for COVID-19 prevention or treatment.

# Materials And Methods

### Extract preparation

High CBD *Cannabis sativa* strain Arbel (IMC, Israel) inflorescence was extracted using ethanol as previously described[38] and decarboxylated by heating the dried crude extract to 220 °C for 10 minutes. The dried decarboxylated extract was weighed, and then resuspended in absolute methanol (volume of solvent added according to the desired concentration) and filtered through a 0.45 µm syringe filter.

## Extract fractionation

A flash chromatography apparatus equipped with a diode array detector was used to fractionize the decarboxylated crude extract. An Ecoflex C-18 80g (Flash Pure, Buchi, C-18, 50 µm spherical, max. pressure 180 psi) column was used for separation, with methanol and water as the mobile phase as suggested by the manufacturer.

## Chemical analyses

High performance liquid chromatography (HPLC) and gas chromatograph with mass selective detector (GCMS 8860 and GC/MSD 5977B, Agilent) analysis was carried out as previously described[38]. Qualitative and quantitative analysis of phytocannabinoid in fractions was done in comparison to the standard calibration curves obtained from dissolving standards in methanol at different concentrations from 0-25 µg/mL.

## Standard/material preparation

The cannabinoid standards in concentration of 1 mg/mL in methanol used in this study included cannabidiol (CBD, Restek catalog no. 34011) cannabigerol (CBG, Restek catalog no. 34091) and tetrahydrocannabivarin (THCV, Restek catalog no. 34100). Inverse agonists (IA) to cannabinoid receptors type 1 (CB1) and 2 (CB2) used were Abcam products: CB1 (AM251, ab120088), CB2 (SR144528, ab146185) and TRPA1 blocker (HC-030031, ab120554), all dissolved in DMSO at a concentration of 10 mM. Phorbol 12-myristate 13-acetate (PMA) (P1585; Sigma Aldrich, USA) was dissolved in DMSO at the stock concentration of 5 µg/mL. Dexamethozone (D4902; Sigma Aldrich, USA) was dissolved in methanol at the stock concentration of 1000 µg/mL. Ruxolitinib JAKAVI was dissolved in DMSO at the concentration of 5000 µg/mL, confirmed with GCMS and HPLC. TNFα (300-01A; PeproTech, Rocky Hill, NJ, USA) was dissolved in water at the stock concentration of 100 µg/mL. (3-Aminopropyl) triethoxysilane (APTES), N-(3-Dimethylaminopropyl)-N(3-ethylcarbodiimide hydrochloride (EDC), and 5(6)-Carboxyfluorescein, 2-(4- Morpholino) ethanesulfonic acid (MES) were purchased from Sigma-Aldrich (USA). Analytical grade methanol and ultra-pure deionized water (MS grade) were used as received without further purification. Palmitic acid (Sigma Aldrich; P0500, USA) was dissolved in methanol at the stock concentration of 0.5 mol/L and used at 150 µM.

## Cell cultures

The lung cancer cell line A549 (ATCC® CCL-185™) was cultured in DMEM (01-055-1A, Biological Industries, Israel) growth media supplemented with 10% FBS, 1% Glutamic acid, 1% pen-strep and plasmocin. Macrophage cell line KG1 (ATCC® CCL-246™) was cultured in IMDM (01-058-1A; Biological Industries, Israel) containing 20% FBS and 1% pen-strep and plasmocin. 10 ng/mL PMA in IMDM media supplemented with 5% FBS, 1% pen-strep and plasmocin was used as stimulating environment for the differentiation of KG1 cells. Differentiated cells with typical morphology were attached to the plate surface within 1-2 days of initiation[39].

## Determination of IL levels and cell viability

IL-6 and IL-8 levels were determined as described previously[40] with the following modifications: A549 cells were plated at 5 x $10^4$ cells per well in DMEM complete media (400 µL) in 24-well cell culture plate. They were allowed to attach and grow at 37 °C in air and 5% $CO_2$ in a humidified incubator overnight with complete DMEM, and then the media was replaced with serum free DMEM for on. Following, cell excitation was performed with 300 ng/mL TNFα. Treatments were performed with plant extract, fraction/compounds given together with 100 µL serum free DMEM. IL-6 and IL-8 secretion levels were analyzed after 4 h of incubation. Supernatant samples were taken and tested using IL-6 and IL-8 ELISA kits (DY206 and DY208 respectively, R&D Systems, Minneapolis, MN, USA). Dexamethasone was used as a positive control. For cell viability, an Alamar Blue (resazurin) assay was performed on each well as described previously[40]. For dose response assays, data points were connected by non-linear regression lines of the sigmoidal dose-response relation. GraphPad Prism (GraphPad Software Inc., San Diego, USA) was employed to produce dose-response curves and IC50 doses were calculated using nonlinear regression analysis.

## Salinization of silicon dioxide surfaces with APTES

To prepare the silica dispersion 1 g of silica was added to 40 mL of methanol and stirred. Then, APTES (0.0045 moles) was slowly added to the solution. The reaction was carried out at ambient temperature for 45 min. After silanization, 50-100 nm or 30-70 nm particles were collected by centrifugation (9000 rpm, 10 min) washed 4 times with water, and dried at 35 °C under vacuum for 3 h [41].

## Labeling of amine functionalized silica nanoparticles with 5(6)-Carboxyfluorescein and IgG

Stock solutions of 1 mg of EDC were prepared separately in 1 mL of 0.1 M MES (pH 4.5-5) buffer. 100 mg of the amine functionalized silica nanoparticles were added to 600 µL of the MES buffer followed by 200 µL of the EDC. The mixture was vortexed for 10 min. Then 100 µL 5(6)-Carboxyfluorescein (1mg/mL) only (for 50-100 nm SNP or 30-70 nm ENP nanoparticles) or 100 µL 5(6)-Carboxyfluorescein (1mg/mL) and IgG (10mg/mL; for 30-70 nm ENPG nanoparticles) solutions were added. The final solution was then mixed by vortex for 3 h at ambient room temperature. Subsequently, the mixture was centrifuged and rinsed with MES buffer to remove excess reactants. EDC was used as a cross-linker to chemically attach the carboxyl group of the 5(6)-Carboxyfluorescein molecule and producing an amine-reactive O-acylisourea. For the fluorescent-IgG labelled silica nanoparticles this intermediate product reacted with the amino groups of the silica nanoparticles to yield an amide bond, releasing fluorescent-IgG labelled silica nanoparticles and urea as a by-product[42]. The fluorescent labelled (SNP or ENP) or fluorescent-IgG labelled (ENPG) silica nanoparticles were then dispersed again in the MES buffer for further analysis.

## Cellular staining and confocal microscopy

Differentiated macrophages from KG1 cells ($10x10^4$ cells/plate; plated on the bottom of a glass cell culture dish) were incubated in 500 uL of 5% FBS-IMDM media with SNP or SNPG (40 µg/mL) and incubated at 37 °C for 4 h for phagocytosis. Macrophages that underwent phagocytosis were fixed with 3.7% formaldehyde solution and permeabilized with 0.1% Triton X-100 at room temperature. Fixed cells were blocked in PBS containing 1% bovine serum albumin. Cells were incubated with EasyProbes™ ActinRed 555 Stain for actin and Hoechst for nuclear staining (AP-FP032, GC-C057 respectively; ABP Bioscience Rockville, MD, USA). Cell microscopy and image acquisition was carried out using a Leica SP8 laser scanning microscope (Leica, Wetzlar, Germany), equipped with a 405, 488 and 552 nm solid state lasers, HCX PL APO CS 10x/0.40 or HC PL APO CS 63x/1.2 water immersion objective (Leica, Wetzlar, Germany) and Leica Application Suite X software (LASX, Leica, Wetzlar, Germany). Hoechst, 5(6)-Carboxyfluorescein and ActinRed 555 emission signals were detected with PMT and HyD (hybrid) detectors in ranges of 415–490 nm, 500-535 nm and 565–660 nm, respectively.

## Quantitative real-time (qRT) PCR

qRT PCR was done as described[38]. Briefly, cells were treated with cannabis compounds or methanol as vehicle control for 6 h. Cells were then harvested and total RNA was extracted. RNA was reverse-transcribed, primers were designed and PCR was performed. The expression of each target gene was normalized to the expression of *Hypoxanthine Phosphoribosyltransferase 1* (*HPRT1*) mRNA in the $2^{-\Delta\Delta Ct}$ and is presented as the ratio of the target gene to HPRT mRNA, expressed as $2^{-\Delta Ct}$, where Ct is the threshold cycle and ΔCt = Ct Target - Ct HPRT1. Experiments were repeated three times. The primers were:

*ACE2* (Gene ID: 59272) (forward) 5’-AAGCACTCACGATTGTTGGG-3’ (reverse) 5’-CACCCCAACTATCTCTCGCT -3’;

*CCL2* (Gene ID: 6347) (forward) 5’- AAGGAGATCTGTGCTGACCC -3’ (reverse) 5’-GCTGCAGATTCTTGGGTTGT -3’;

*IL-6* (Gene ID: 3569) (forward) 5’- GAACTCCTTCTCCACAAGCG -3’ (reverse) 5’-GAAGAGGTGAGTGGCTGTCT -3’;

*CCL7* (Gene ID: 6354) (forward) 5’- CACCCTCCAACATGAAAGCC -3’ (reverse) 5’-GGTGGTCCTTCTGTAGCTCT -3’;

*IL-7* (Gene ID: 3574) (forward) 5’- CTGAAAGTACACTGCTGGCG -3’ (reverse) 5’-GAGTTGCCGAGTCTGTGTTG3’;

*FCγR2A* (Gene ID: 2212) (forward) -5’-GCC AAT TCC ACT GAT CCT GT-3’

(reverse) - 5’- CCTGGGGTTCAGAGTCATGT -3’;

*SCARB1* (Gene ID: 949) (forward) -5’-CTG TGG GTG AGA TCA TGT GG-3’

(reverse)- 5’-GTT CCA CTT GTC CAC GAG GT-3’;

*CD36* (Gene ID: 948 ) (forward) -5’-AGA TGC AGC CTC ATT TCC AC -3’

(reverse)-5’-TGG GTT TTC AAC TGG AGA GG -3’;

*IL-8* (Gene ID: 3576) (forward) -5’-CAG GAA TTG AAT GGG TTT GC -3’

(reverse)-5’-AAA CCA AGG CAC AGT GGA AC -3’.

## Imaging Flow Cytometry

Differentiated macrophages from KG1 cells ($10x10^5$ cells/plate; seeded on 6-well plate culture dish) were replaced with 2 mL of 5% FBS-IMDM media with SNP, ENP, or ENPG (40 µg/mL) and incubated at 37 °C for 4 h for phagocytosis. The cells were detached from the surface of the plate using a trypsin 0.25% : EDTA 0.05% solution (03-052-1A, Biological Industries, Israel) for 3 min, washed with DMEM complete media, centrifuged and transferred to 50 uL cold PBS kept on ice.

Cells were analyzed by multispectral imaging flow cytometry (ImageStream markII flow cytometer; Amnis Corp, part of EMD Millipore, Seattle, WA, USA). Fluorescence intensity of the Fluorescein labeled silica beads was measured in channel 2 of the cytometer (480 nm ex, 560 nm em). A X60 magnification was used for all samples. At least 4,000 cells were collected for each sample and data were analyzed using a

dedicated image analysis software (IDEAS 6.2; AmnisCorp). Cells were gated for single cells using the area and aspect ratio features, and for focused cells using the Gradient RMS feature. Cropped cells were further eliminated by plotting the cell area of the bright field image against the Centroid X feature (the number of pixels in the horizontal axis from the left corner of the image to the center of the cell mask). Cells were further gated for cells that were positive (for ENP, ENPG or SNP). Because of their larger size only SNP beads could be further analyzed for beads internalization vs. those attached to the cell surface. The was done using the intensity feature (the sum of the background – subtracted pixel values within the masked area of the image) and max pixel (the largest value of the background subtracted pixel). SNP internalization was calculated by the internalization feature, i.e. the ratio of the intensity inside the cell to the intensity of the entire cell, mapped to a log scale. To define the internal mask for the cell, the object mask of the brightfield image was eroded by 8 pixels. Cells with an internalization score higher than 0.33 were gated as cells with internalized SNP.

### Statistical analysis

The data were processed using JMP statistical package (SAS Inc, NC, USA). Comparisons between two groups were made with the Student's T-Test. Comparisons between more than 2 groups were made with two-way analysis of variance (ANOVA) followed by Tukey-Kramer's honest significant difference (HSD) test as post hoc. Values are shown as mean ± standard error (s.e.m.). $P$ values $\leq 0.05$ were considered significant.

## Declarations


### Acknowledgements

We thank Zach Dunseth for English editing.


### Author contributions

S.M.A., S.N. and A.C.V. conducted experiments, N.S. designed experiments and analyzed the results, S.A. conducted experiments, D.N. performed chemical analysis, E.B. performed microscopy examination, I.S. performed ImageStream analysis, K.A.M. was in charge of particle formation, G.M. managed particle formation and was involved with project conception, H.K. conceived the project, supervised the experiments and analysis, and wrote the manuscript. All authors read and approved the final draft of the manuscript.

### Authors declare no conflict of interest

## References

1. Mehta, P. *et al.* COVID-19: consider cytokine storm syndromes and immunosuppression. *Lancet (London, England)* **395**, 1033 (2020).
2. Shi, Y., et al., COVID-19 infection: the perspectives on immune responses. *Cell Death Differ.* **27**, 1451–1454 (2020).
3. Ruscitti, P., Berardicurti, O., Iagnocco, A. & Giacomelli, R. Cytokine storm syndrome in severe COVID-19. *Autoimmun. Rev.* **19**, 102562 (2020).
4. Gao, Y. *et al.* Diagnostic utility of clinical laboratory data determinations for patients with the severe COVID-19. *J. Med. Virol.* **92**, 791–796 (2020).
5. Hanuš, L. O., Meyer, S. M., Muñoz, E., Taglialatela-Scafati, O. & Appendino, G. Phytocannabinoids: a unified critical inventory. *Nat. Prod. Rep.* **33**, 1357-1392 (2016).
6. Berman, P. *et al.* A new ESI-LC/MS approach for comprehensive metabolic profiling of phytocannabinoids in Cannabis. *Sci. Rep.* **8**, 1-15 (2018).
7. Aizpurua-Olaizola, O. *et al.* Evolution of the cannabinoid and terpene content during the growth of *Cannabis sativa* plants from different chemotypes. *J. Nat. Prod.* **79**, 324-331 (2016).
8. Oláh, A., Szekanecz, Z. & Bíró, T. Targeting cannabinoid signaling in the immune system: “High”-ly exciting questions, possibilities, and challenges. *Front. Immunol.* **8**, 1487 (2017).
9. Gonçalves, E. D. & Dutra, R. C. Cannabinoid receptors as therapeutic targets for autoimmune diseases: where do we stand? *Drug Discov. Today* **24**, 1845-1853 (2019).
10. Romano, B. *et al.* Pure Δ9-tetrahydrocannabivarin and a *Cannabis sativa* extract with high content in Δ9-tetrahydrocannabivarin inhibit nitrite production in murine peritoneal macrophages. *Pharmacol. Res.* **113**, 199-208 (2016).
11. Friedman, M., Cepero, M. L., Klein, T. & Friedman, H. Suppressive effect of Δ9-tetrahydrocannabinol in vitro on phagocytosis by murine macrophages. *Proc. Soc. Exp. Biol. Med.* **182**, 225-228 (1986).
12. Ahmed, A. *et al.* Ruxolitinib in adult patients with secondary haemophagocytic lymphohistiocytosis: an open-label, single-centre, pilot trial. *Lancet Haematol.* **6**, e630-e637 (2019).
13. Hua, W. *et al.* CD36 mediated fatty acid-induced podocyte apoptosis via oxidative stress. *PloS ONE* **10**, e0127507 (2015).
14. Gallily, R., Yekhtin, Z. & Hanuš, L. O. Overcoming the bell-shaped dose-response of cannabidiol by using cannabis extract enriched in cannabidiol. *Pharmacol. Pharm.* **6**, 75 (2015).
15. Laprairie, R., Bagher, A., Kelly, M. & Denovan-Wright, E. Cannabidiol is a negative allosteric modulator of the cannabinoid CB1 receptor. *Br. J. Pharmacol.* **172**, 4790-4805 (2015).
16. Mukhopadhyay, I. *et al.* Expression of functional TRPA1 receptor on human lung fibroblast and epithelial cells. *J. Recept. Signal Transduct. Res.* **31**, 350-358 (2011).
17. Merad, M. & Martin, J. C. Pathological inflammation in patients with COVID-19: a key role for monocytes and macrophages. *Nat. Rev. Immunol.* **20**, 355–362 (2020).
18. Remy, K. E. *et al.* Immunotherapies for COVID-19: lessons learned from sepsis. *Lancet Respir. Med.* (2020). https://dx.doi.org/10.1016%2FS2213-2600(20)30217-4

19. Levy, Y. *et al.* Enhanced T cell recovery in HIV-1–infected adults through IL-7 treatment. *J. Clin. Invest.* **119**, 997-1007 (2009).
20. Dalan, R.; *et al*. The ACE-2 in COVID-19: Foe or friend? *Horm. Metab. Res.* **52**, 257 (2020).
21. Li, F., Li, W., Farzan, M. & Harrison, S. C. Structure of SARS coronavirus spike receptor-binding domain complexed with receptor. *Science* **309**, 1864-1868 (2005).
22. Garvin, M. R. *et al.* A mechanistic model and therapeutic interventions for COVID-19 involving a RAS-mediated bradykinin storm. *elife* **9**, e59177 (2020).
23. Wang, C. *et al.* Alveolar macrophage dysfunction and cytokine storm in the pathogenesis of two severe COVID-19 patients. *EBioMedicine* **57**, 102833 (2020).
24. Merad, M. & Martin, J. C. Pathological inflammation in patients with COVID-19: a key role for monocytes and macrophages. *Nat. Rev. Immunol.* **20**, 1-8 (2020).
25. Yoshikawa, T., Hill, T., Peters, C. J. & Tseng, C.-T. K. Severe acute respiratory syndrome-Coronavirus (SARS-CoV)-induced lung epithelial cytokines exacerbate SARS pathogenesis by modulating intrinsic functions of monocyte-derived macrophages and dendritic cells. *J. Virol.* (2008). https://doi.org/10.1128/JVI.01792-08
26. Yasui, F. *et al.* Phagocytic cells contribute to the antibody-mediated elimination of pulmonary-infected SARS coronavirus. *Virology* **454**, 157-168 (2014).
27. Horsthemke, M. *et al.* Multiple roles of filopodial dynamics in particle capture and phagocytosis and phenotypes of Cdc42 and Myo10 deletion. *J. Biol. Chem.* **292**, 7258-7273 (2017).
28. Tsugita, M., Morimoto, N., Tashiro, M., Kinoshita, K. & Nakayama, M. SR-B1 is a silica receptor that mediates canonical inflammasome activation. *Cell Rep.* **18**, 1298-1311 (2017).
29. Greenberg, S. & Grinstein, S. Phagocytosis and innate immunity. *Curr. Opin. Immunol.* **14**, 136-145 (2002).
30. Wang, X., Lv, L., Chen, Y. & Chen, J. A CD36 synthetic peptide inhibits silica-induced lung fibrosis in the mice. *Toxicol. Ind. Health* **26**, 47-53 (2010).
31. He, W. *et al.* Alveolar macrophages are critical for broadly-reactive antibody-mediated protection against influenza A virus in mice. *Nat. Commun.* **8**, 1-14 (2017).
32. Huber, V. C., Lynch, J. M., Bucher, D. J., Le, J. & Metzger, D. W. Fc receptor-mediated phagocytosis makes a significant contribution to clearance of influenza virus infections. *J. Immunol.* **166**, 7381-7388 (2001).
33. Cooper, G. E. et al. Viral inhibition of bacterial phagocytosis by human macrophages: redundant role of CD36. *PLoS One* **11**, e0163889 (2016).
34. Yip, M. S. *et al.* Antibody-dependent infection of human macrophages by severe acute respiratory syndrome coronavirus. *Virol. J.* **11**, 1-11 (2014).
35. Merad, M. & Martin, J. C. Pathological inflammation in patients with COVID-19: a key role for monocytes and macrophages. *Nat. Rev. Immunol.* **20**, 355–362(2020).

36. Navarro, S., Debili, N., Bernaudin, J., Vainchenker, W. & Doly, J. Regulation of the expression of IL-6 in human monocytes. *J. Immunol.* **142**, 4339-4345 (1989).
37. Pastor, F. P., Folgar, M. I., Carvalho, N., Carvalho, F. & Horcajadas, F. A. Therapeutic Cannabis and COVID-19: between opportunism and infoxication. *Adicciones* **32**, 167-172 (2020).
38. Mazuz, M., *et al.* Synergistic cytotoxic activity of cannabinoids from cannabis sativa against cutaneous T-cell lymphoma (CTCL) in-vitro and ex-vivo. *Oncotarget* **11**, 1141 (2020).
39. Starr, T., Bauler, T. J., Malik-Kale, P. & Steele-Mortimer, O. The phorbol 12-myristate-13-acetate differentiation protocol is critical to the interaction of THP-1 macrophages with *Salmonella* typhimurium. *PLoS ONE* **13**, e0193601 (2018).
40. Nallathambi, R. *et al.* Anti-inflammatory activity in colon models is derived from δ9-tetrahydrocannabinolic acid that interacts with additional compounds in cannabis extracts. *Cannabis Cannabinoid Res.* **2**, 167-182 (2017).
41. Yaakov, N. *et al.* Single cell encapsulation via pickering emulsion for biopesticide applications. *ACS omega* **3**, 14294-14301 (2018).
42. Mani, K. A., Yaakov, N., Itzhaik Alkotzer, Y., Zelikman, E. & Mechrez, G. A robust fabrication method for amphiphilic Janus particles via immobilization on polycarbonate microspheres. *Polymers* **10**, 900 (2018).

# Figures

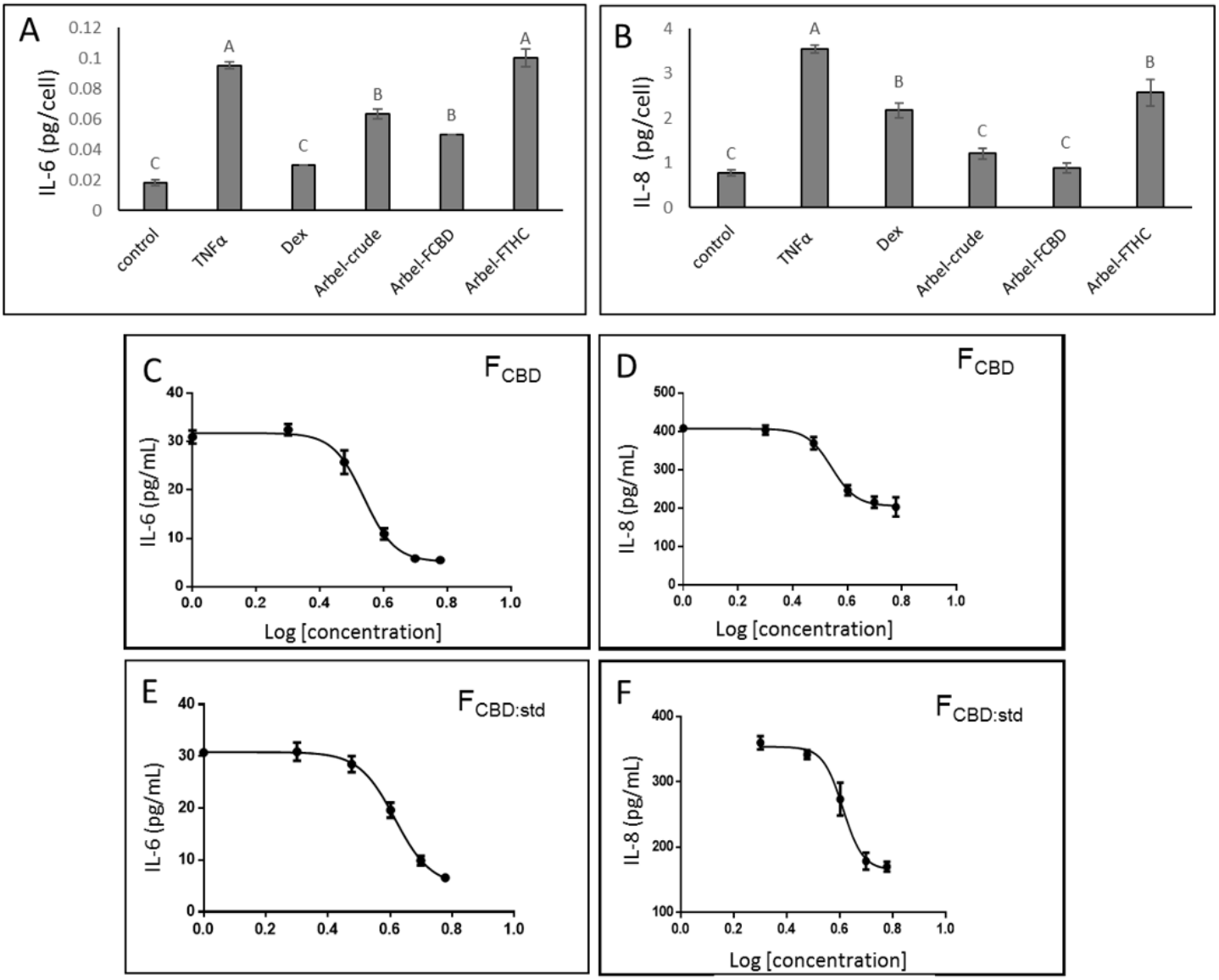


## Figure 1

The level of (A) IL-6 and (B) IL-8 in A549 cells treated with crude and different fractions of C. sativa Arbel extract. Cells were treated with 300 ng/mL TNFα and C. sativa extract and fractions at a concentration of 5 µg/mL for 4 h. IL-6 and IL-8 levels were measured from the supernatant. Values (pg/cell) were calculated relative to a TNFα-treated control and normalized to cell number as determined in Alamar Blue fluorescence (resazurin) assay. Dexamethasone (Dex; 4 µg/mL) served as a positive control. Control (methanol) treatment served as solvent (vehicle) control; TNFα is TNFα+methanol treatment control. Error bars indicate ± s.e.m. (n = 3). Levels with different letters are significantly different from all combinations of pairs by Tukey-Kramer honest significant difference (HSD; $P \leq 0.05$). (C,D) Dose-effect curves of C. sativa FCBD on IL-6 or IL-8 levels, respectively, in A549 cell line. (E,F) Dose-effect curves of FCBD:std (CBD+CBG+THCV; 93.5, 6.1, 0.4%, respectively) on IL-6 and IL-8 levels, respectively, in A549 cell line. Data points were connected by non-linear regression lines of the sigmoidal dose-response relation. GraphPad Prism was used to produce the dose-response curve and IC50 doses. Error bars indicate ± s.e.m. (n = 3).

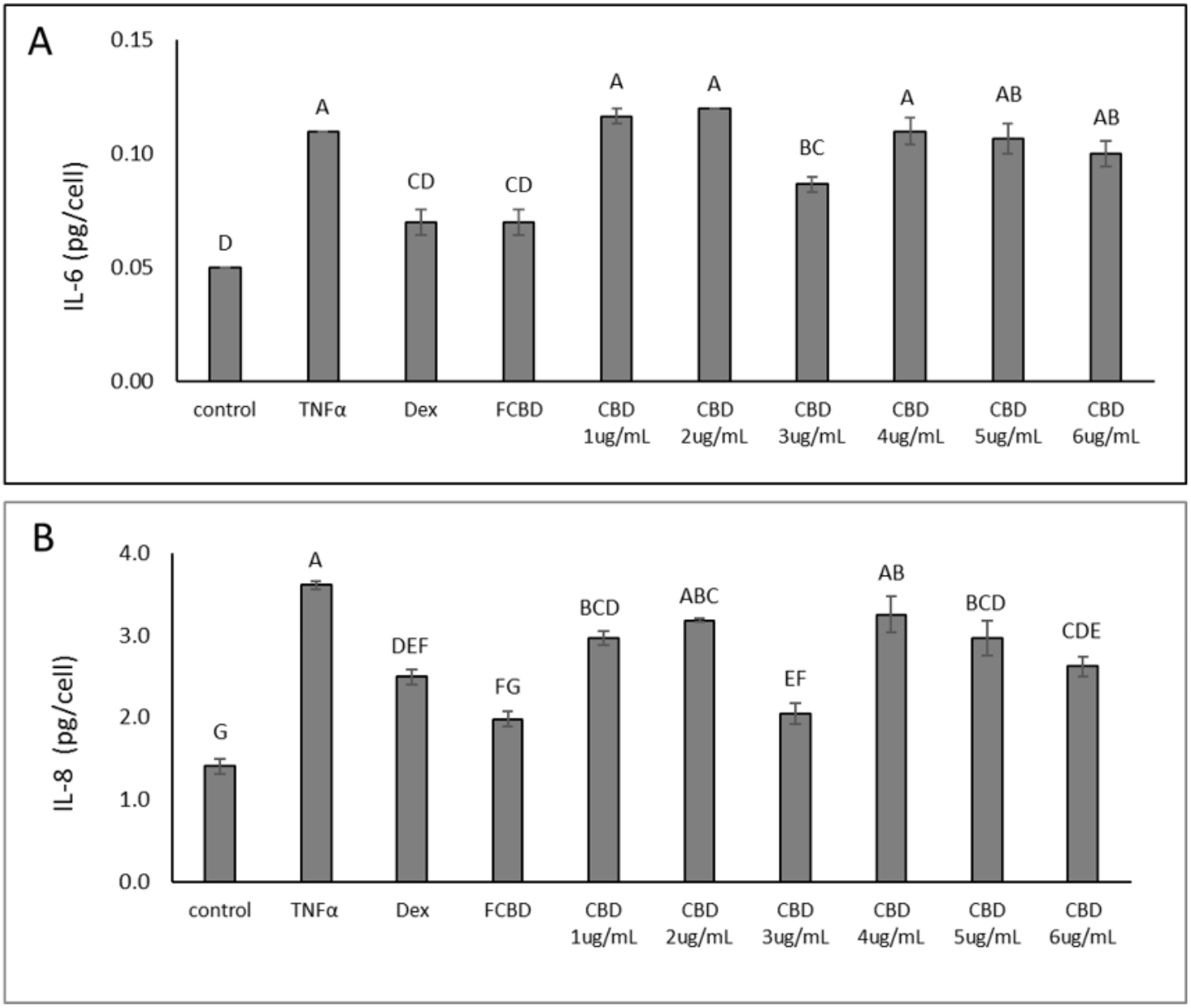


## Figure 2

The level of (A) IL-6 and (B) IL-8 in A549 cells treated with FCBD and CBD. Cells were treated with 300 ng/mL TNFα, 4.1 µg/mL FCBD (FCBD) and CBD at different concentrations for 4 h. IL-8 or IL-6 levels were measured from the supernatant. Values (pg/cell) were calculated relative to a TNFα-treated control and normalized to cell number as determined in Alamar Blue fluorescence (resazurin) assay. Dexamethasone (Dex; 4 µg/mL) served as a positive control. Control (methanol) treatment served as solvent (vehicle) control; TNFα is TNFα+methanol treatment control. Error bars indicate ± s.e.m. (n = 3). Levels with different letters are significantly different from all combinations of pairs by Tukey-Kramer honest significant difference (HSD; $P \leq 0.05$).

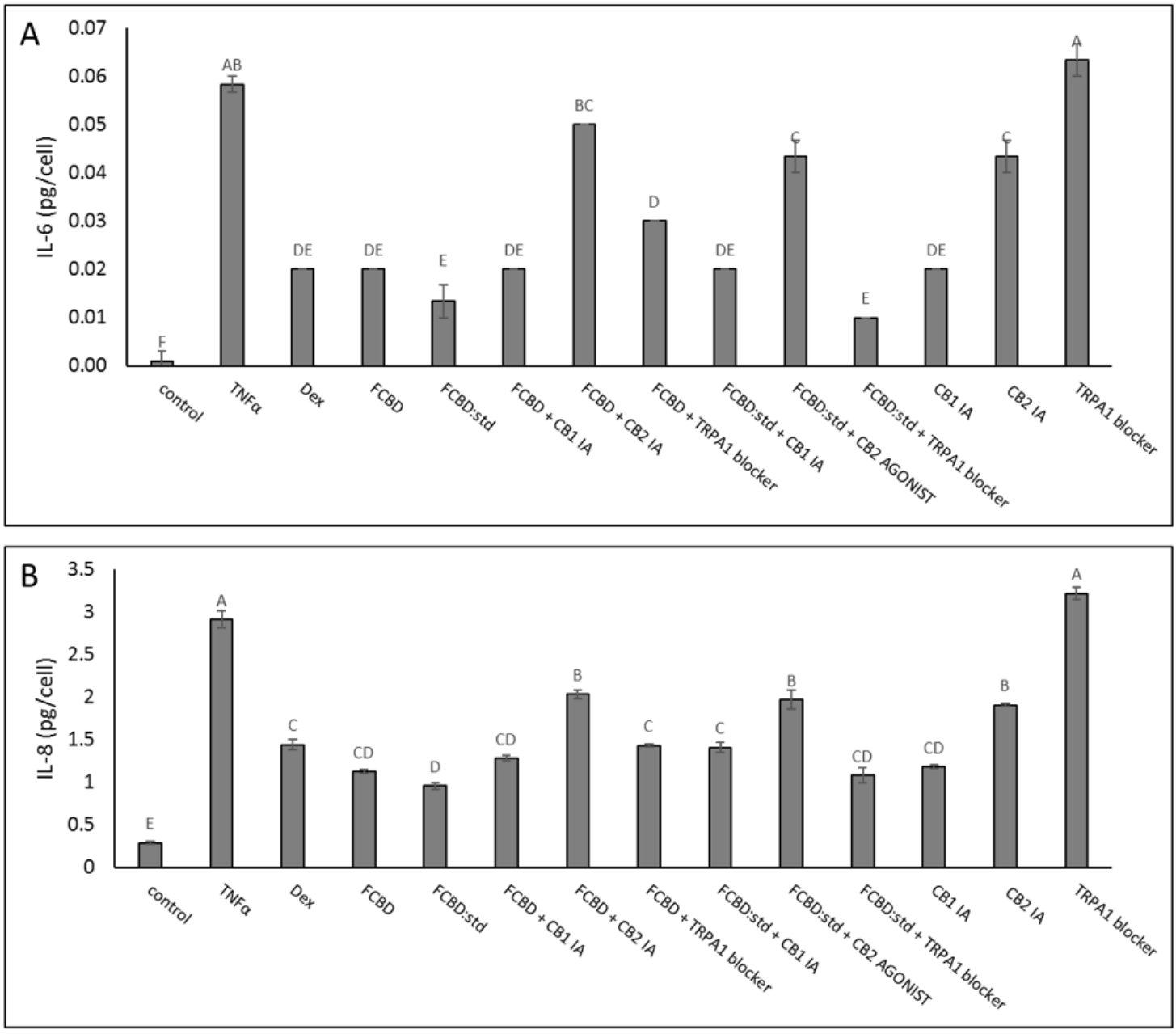


## Figure 3

The level of (A) IL-6 and (B) IL-8 in A549 cells treated with FCBD and FCBD-std with or without CB1 or CB2 inverse agonists (IA) or TRPA1 blocker. Cells were treated with 300 ng/mL TNFα and FCBD (FCBD) and FCBD-std (FCBD-std) at a concentration of 3.4 and 4.1 µg/mL, respectively, in the presence or absence of IA of CB1 or CB2 or a TRPA1 blocker, for 4 h. IL-6 and IL-8 levels were measured from the supernatant. Values (pg/cell) were calculated relative to a TNFα-treated control and normalized to cell number as determined via Alamar Blue fluorescence (resazurin) assay. Dexamethasone (Dex) served as a positive control at 4 µg/mL. Control (methanol) treatment served as solvent (vehicle) control; TNFα is TNFα+methanol treatment control. Error bars indicate ± s.e.m. (n = 3). Levels with different letters are significantly different from all combinations of pairs by Tukey-Kramer honest significant difference (HSD; $P \leq 0.05$).

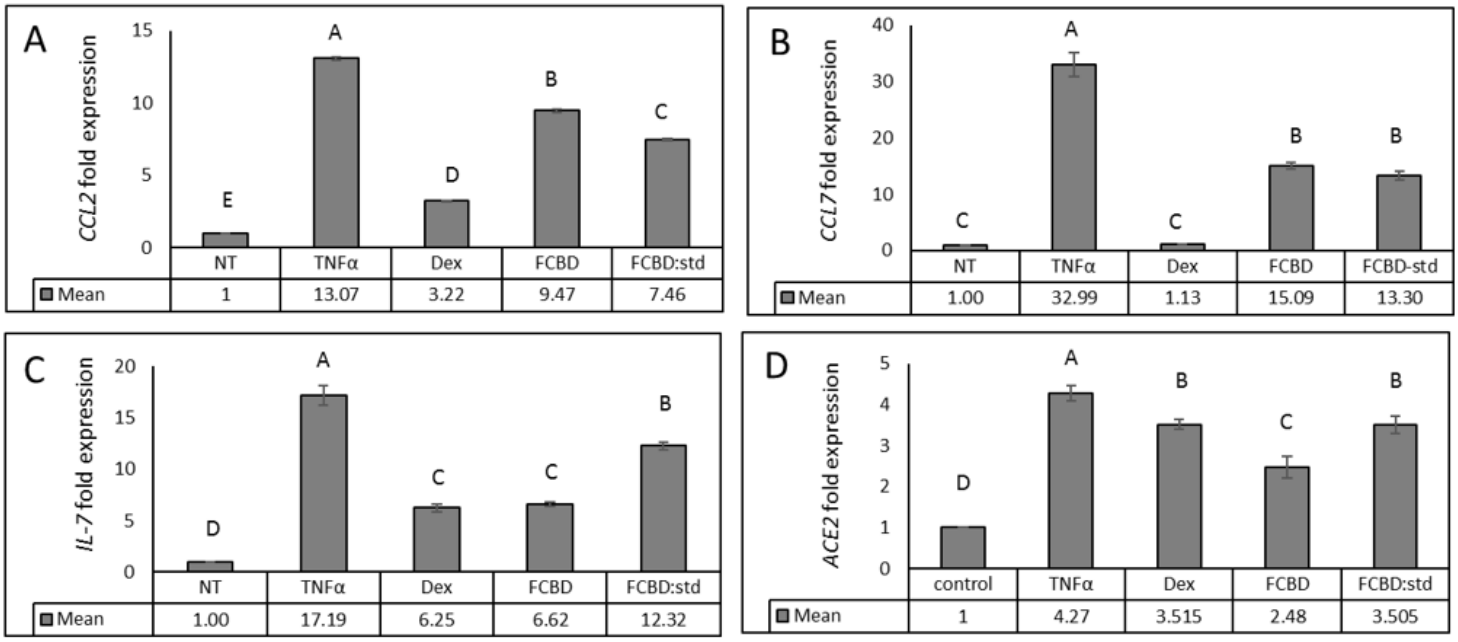


## Figure 4

Quantitative PCR-based determination of the RNA steady state level in A549 cell line of (A) CCL2, (B) CCL7, (C) IL-7 or (D) ACE2 genes, after treatment with TNFα (300 µg/mL) and FCBD (FCBD) at 7 µg/mL, or Dexamethasone (Dex) 4 µg/mL - for 6 h relative to control. Gene transcript values were determined by quantitative PCR as a ratio between the target gene versus a reference gene (HYPOXANTHINE PHOSPHORIBOSYLTRANSFERASE1; HPRT1; geneID 3251). Values were calculated relative to the average expression of target genes in treated versus control using the 2ΔΔCt method. Error bars indicate ± s.e.m. (n = 3). Levels with different letters are significantly different from all combinations of pairs by Tukey-Kramer honest significant difference (HSD; $P \leq 0.05$).

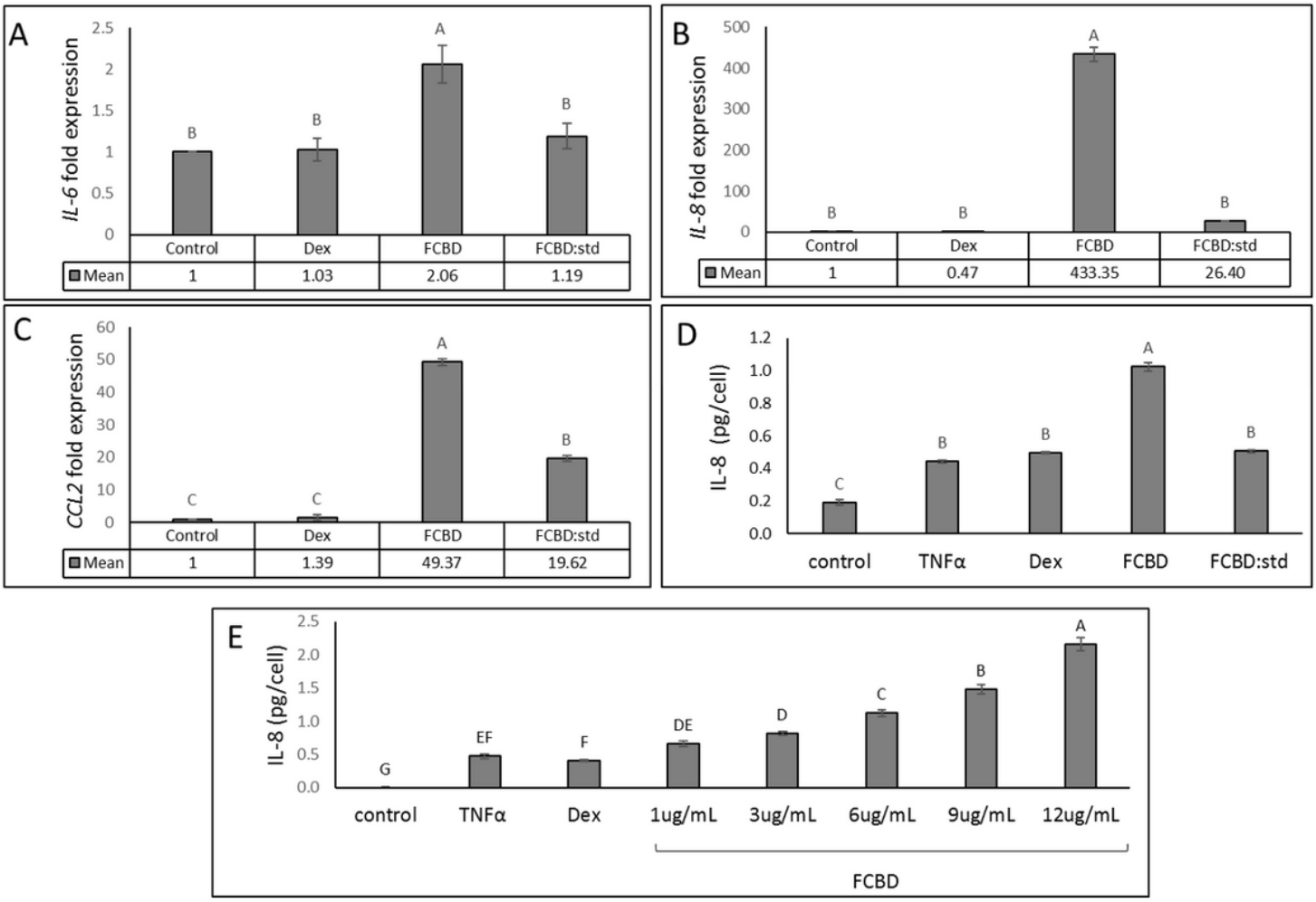


## Figure 5

(A,B,C) Quantitative PCR-based determination of the RNA steady state level in differentiated KG1 cell line of (A) IL-6, (B) IL-8 or (C) CCL2 after treatment with FCBD (FCBD) at 7 µg/mL, FCBD:std (FCBD:std) at 7 µg/mL or Dexamethasone (Dex) at 8 µg/mL for 6 h relative to control. Gene transcript values were determined by quantitative PCR as a ratio between the target gene versus a reference gene (HYPOXANTHINE PHOSPHORIBOSYLTRANSFERASE1; HPRT1; geneID 3251). Values were calculated relative to the average expression of target genes in treated versus control using the 2ΔΔCt method. (D,E) The level of IL-8 in KG1 cells treated with FCBD and FCBD-std. Cells were treated with 300 ng/mL TNFα (and not by PMA), FCBD (FCBD) or FCBD:std (FCBD:std) at 10 µg/mL (D) or at different concentrations of FCBD-std (E) for 4 h. IL-8 level was measured from the supernatant. Values (pg/cell) were calculated relative to a TNFα-treated control and normalized to cell number as determined in Alamar Blue fluorescence (resazurin) assay. Dexamethasone (Dex; 4 µg/mL) served as a positive control. Control (methanol) treatment served as solvent (vehicle) control; TNFα is TNFα+methanol treatment control. Error bars indicate ± s.e.m. (n = 3). Levels with different letters are significantly different from all combinations of pairs by Tukey-Kramer honest significant difference (HSD; $P \leq 0.05$).

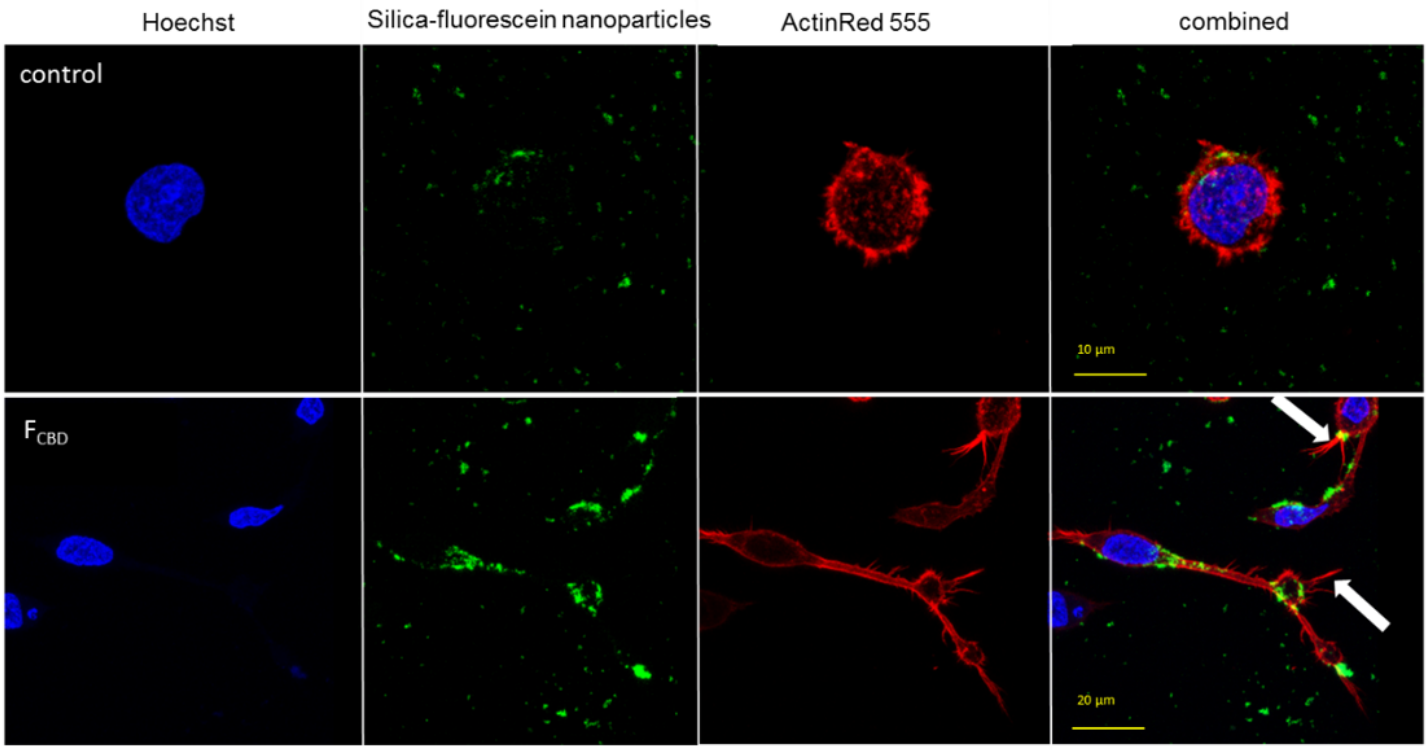


## Figure 6

Representative examples of confocal images of macrophages following treatment with FCBD (7 µg/mL) and solvent (vehicle) control. Differentiated KG1 cells were treated with FCBD or control for 16 h and then incubated with silica beads (SNP; 40 µg/mL) for 4 h. Cell were stained for F-actin (EasyProbes™ ActinRed 555 Stain, red stain), and nuclei (Hoechst, blue stain); n ≥ 5, in each biological replicate multiple cells were examined (see Table 2). Membrane filopodia-like structures are marked with white arrows.

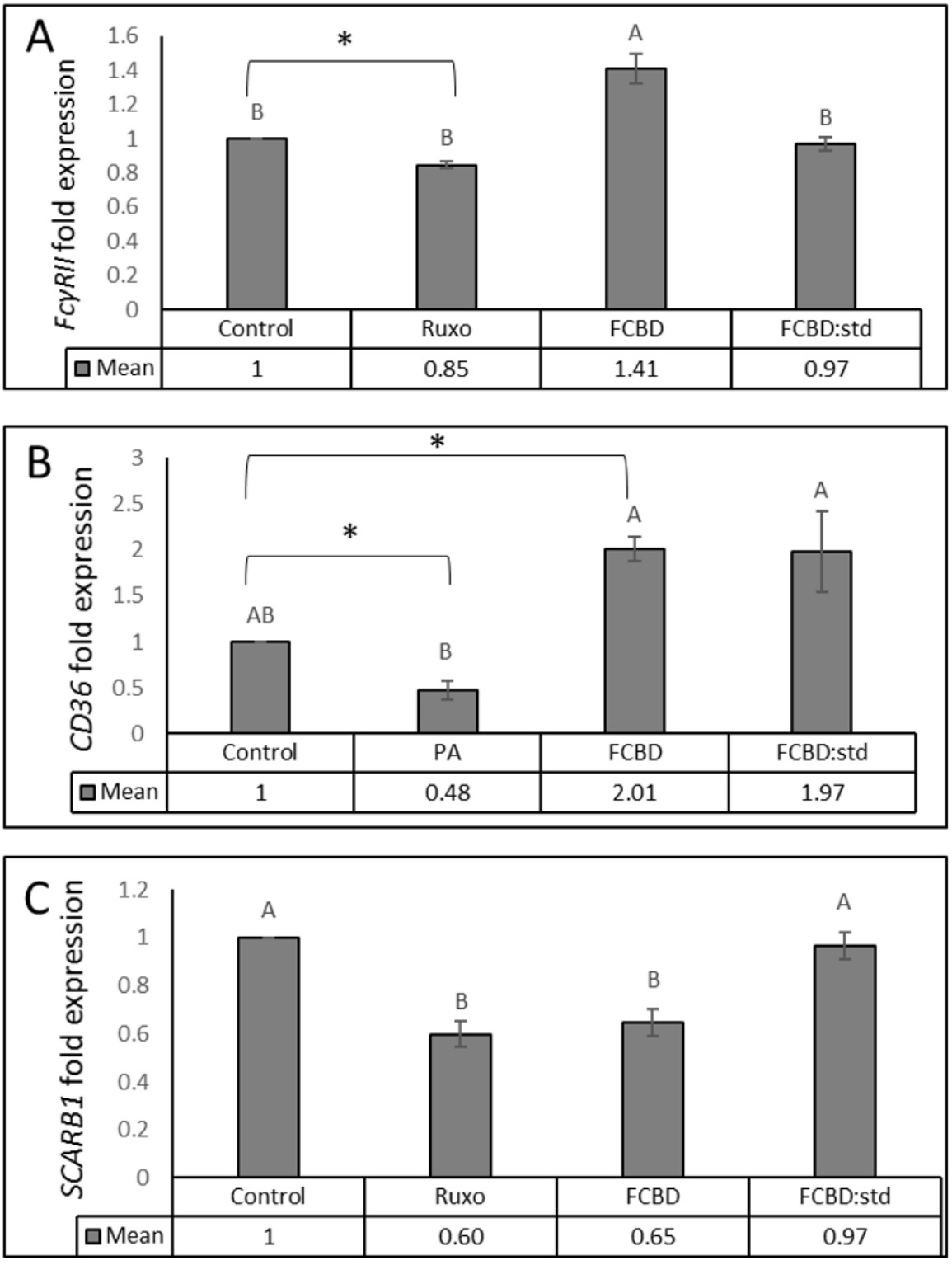


## Figure 7

Quantitative PCR-based determination of the RNA steady state level in differentiated KG1 cell line of (A) FcγRII, (B) CD36 or (C) SCARB1 genes, after treatment with FCBD (FCBD) at 7 µg/mL, FCBD:std (FCBD:std) at 7 µg/mL, Ruxolitinib (Ruxo) at 100 µg/mL or Palmitic acid (PA) at 150 µM. Gene transcript values were determined by quantitative PCR as a ratio between the target gene versus a reference gene (HYPOXANTHINE PHOSPHORIBOSYLTRANSFERASE1; HPRT1; geneID 3251). Values were calculated

relative to the average expression of target genes in treated versus control using the 2ΔΔCt method. Error bars indicate ± s.e.m. (n = 3). Levels with different letters are significantly different from all combinations of pairs by Tukey-Kramer`s honest significant difference (HSD; $P \leq 0.05$). *indicates significantly different mean from the control based on Student T-test ($P \leq 0.05$).

## Supplementary Files

This is a list of supplementary files associated with this preprint. Click to download.

- SI.docx